SCIENTIFIC REP⚙RTS

Anatase TiO_2 Nanoparticles with Exposed {001} Facets for Efficient Dye-Sensitized Solar Cells

Liang Chu[1], Zhengfei Qin[2], Jianping Yang[1] & Xing'ao Li[2]

Anatase TiO_2 nanoparticles with exposed {001} facets were synthesized from Ti powder *via* a sequential hydrothermal reaction process. At the first-step hydrothermal reaction, H-titanate nanowires were obtained in NaOH solution with Ti powder, and at second-step hydrothermal reaction, anatase TiO_2 nanoparticles with exposed {001} facets were formed in NH_4F solution. If the second-step hydrothermal reaction was carried out in pure water, the H-titanate nanowires were decomposed into random shape anatase-TiO_2 nanostructures, as well as few impurity of $H_2Ti_8O_{17}$ phase and rutile TiO_2 phase. Then, the as-prepared TiO_2 nanostructures synthesized in NH_4F solution and pure water were applied to the photoanodes of dye-sensitized solar cells (DSSCs), which exhibited power conversion efficiency (PCE) of 7.06% (V_{OC} of 0.756V, J_{SC} of 14.80 mA/cm^2, FF of 0.631) and 3.47% (V_{OC} of 0.764V, J_{SC} of 6.86 mA/cm^2, FF of 0.662), respectively. The outstanding performance of DSSCs based on anatase TiO_2 nanoparticles with exposed {001} facets was attributed to the high activity and large special surface area for excellent capacity of dye adsorption.

Dye-sensitized solar cells (DSSCs), since the first report by Grätzel in 1991, have captured a lot of attentions due to the advantages of high power conversion efficiency (PCE), low cost, friendly to the environment, and simple fabrication process[1–3]. Traditionally, standard DSSC structure is the combination of photoanodes, dye sensitizers, redox electrolytes, and counter electrodes[4–6]. There, the photoanodes strongly affect the performance of DSSCs, which serve as scaffolds for dye molecules and the transport media for photo-generated electrons[7–10]. As a result, considerable efforts have been devoted to pursuing a more effective photoanode.

Titanium dioxide (TiO_2) is the shared material for photoanode in DSSCs, because of the high chemical and optical stability, low toxicity, and appropriate band structure[11–13]. In DSSCs, the performance profoundly depends upon the morphology, crystalline phase, structure and exposed crystal facet of TiO_2[14–16]. The previous studies indicated that anatase TiO_2 single crystal with exposed {001} facets has good potency for dye adsorption and charge transfer[17]. Both theoretical and experimental studies showed that {001} facets of anatase TiO_2 single crystal are extraordinarily reactive[18], and the surface energy is 0.90 J/m^2, which is much larger than 0.44 J/m^2 surface energy of the usual {101} facets[19]. To date, there have been a large number of reports for preparing anatase TiO_2 single crystal with appropriately exposed {001} facets for application of enhanced DSSCs, such as TiO_2 nanotube[20], anatase TiO_2 nanosheets[21], yolk@shell anatase TiO_2 hierarchical microspheres[22], and mesoporous TiO_2 single crystals[9]. Yet it was reported that the ratio of {001} and {101} facet has impact on the performance of nanodevice because of the "surface heterojunction" of {001} and {101} surfaces, where appropriate but not great proportion of {001} facets is beneficial to the transfer and separation of photogenerated electrons and holes[23,24].

[1]School of Science, Nanjing University of Posts and Telecommunications (NUPT), Nanjing 210046, P. R. China. [2]Key Laboratory for Organic Electronics & Information Displays (KLOEID) & Institute of Advanced Materials (IAM), Jiangsu National Synergistic Innovation Center for Advanced Materials (SICAM), School of Materials Science and Engineering (SMSE), Nanjing University of Posts and Telecommunications (NUPT), Nanjing 210046, P. R. China. Correspondence and requests for materials should be addressed to J.P.Y. (email: yangjp@njupt.edu.cn) or X.A.L.(email: iamxali@njupt.edu.cn)
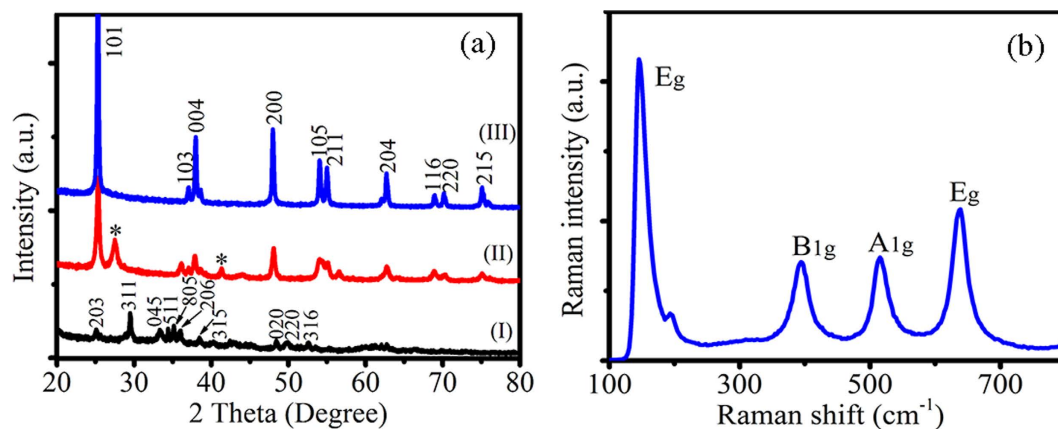
Figure 1. XRD powder patterns and Raman spectroscopy. (**a**) H-titanate nanowires corresponded well to $H_2Ti_5O_{11} \cdot H_2O$ phase (I), the obtained sample after the second-step hydrothermal reaction in pure water was indexed as mainly anatase TiO_2 phase and few $H_2Ti_8O_{17}$ phase and rutile TiO_2 phase (II), the obtained sample in NH_4F solution was indexed as pure anatase TiO_2 phase (III). (**b**) Raman spectroscopy was taken to calculate the percentage of {001} facets as 34% by the peak intensity ratio of the E_g (at 144 cm^{-1}) and A_{1g} (at 514 cm^{-1}) peaks.

Nowadays, the efficiency of DSSCs has been achieved 13% through the molecular engineering of porphyrin sensitizers[25]. It's worth noting that the photoanode is TiO_2 nanoparticle film because of the large specific surface area for loading dye molecules. To the best of our knowledge, it is a challenge to synthesize TiO_2 nanoparticles with appropriately exposed {001} facets, which is the desired material for photoanodes of DSSCs. In this work, anatase TiO_2 nanoparticles with 34% exposed {001} facets were synthesized *via* a two-step hydrothermal reaction method from Ti powder, which were further developed as efficient photoanodes for DSSCs. The first-step hydrothermal reaction of Ti powder in NaOH solution led to the formation of H-titanate nanowires after washing with HCl solution[26], and the second-step hydrothermal reaction resulted in the formation of anatase TiO_2 nanoparticles with exposed {001} facets in NH_4F solution or random shape TiO_2 nanostuctures with tiny impurity phase in pure water. Subsequently, the obtained TiO_2 nanostructures were utilized as photoanodes of DSSCs, yielding PCE of 7.06% (V_{OC} of 0.756 V, J_{SC} of 14.80 mA/cm^2, FF of 0.631) and 3.47% (V_{OC} of 0.764 V, J_{SC} of 6.86 mA/cm^2, FF of 0.662), respectively. The result indicated the anatase TiO_2 nanoparticles with 34% exposed {001} facets possess the characteristics of high activity and large special surface area for the excellent capacity to load dye molecules.

Results

Structure of anatase TiO_2 nanoparticles. Figure 1(a) shows the powder XRD patterns of the as-grown H-titanate nanowires (I), as well as the obtained TiO_2 nanostuctures synthesized in pure water (II) and in NH_4F solution (III). In curve (I), there are several broadened diffraction peaks, which correspond well to the $H_2Ti_5O_{11} \cdot H_2O$ phase (PCPDFWIN, 44-0130). Thus, the Ti powder was reacted with NaOH solution, after washing with dilute HCl solution, the obtained sample was $H_2Ti_5O_{11} \cdot H_2O$. Taking the $H_2Ti_5O_{11} \cdot H_2O$ nanowires as precursor in the following hydrothermal treatment in pure water, the obtained powder was mainly indexed as anatase TiO_2 phase, as revealed in curve (II). Meanwhile, the another peaks besides anatase TiO_2 phase indicate that the $H_2Ti_5O_{11} \cdot H_2O$ nanowires were not completely decomposed into pure anatase TiO_2 phase. The peaks located at 27.71° and 41.86° were corresponded to (012) and (860) planes of $H_2Ti_8O_{17}$ phase, respectively (PCPDFWIN, 36-0656). While the peaks located at 36.13° and 56.55° were assigned to (101) and (220) planes of rutile TiO_2 phase (PCPDFWIN, 87-0710). More importantly, if the further hydrothermal reaction was taken in NH_4F solution, a pure phase of anatase TiO_2 (PCPDFWIN, 84-1286) was observed as the curve (III). Using the Scherrer equation, the average crystal size of anatase TiO_2 nanostructures obtained in NH_4F solution was about 45 nm estimated from the full width at half maximum of the (101) peak. Since no other diffraction peaks belonging to impurities are observed, suggesting that all the $H_2Ti_5O_{11} \cdot H_2O$ nanowires were completely converted to anatase TiO_2 phase in NH_4F solution. The diffraction peaks of curve (III) are sharper than that of curve (II), indicating the better crystallization and larger crystallites due to the enhanced effect of F^{-25}. The obvious (004) diffraction peak of curve (III) suggests dominant crystal growth along the [001] direction[26], which is typical for anatase TiO_2 nanoparticles with exposed {001} facets. In order to quantitatively analyze the percentage of {001} facets, Raman spectroscopy was carried out as shown in Fig. 1(b)[24,27]. The peaks at 144, 394, 514, and 636 cm^{-1} suggest the typical anatase TiO_2 phase, being consistent with the XRD results. The percentage of {001} facets was calculated as 34% by measuring the peak intensity ratio of the E_g (at 144 cm^{-1}) and A_{1g} (at 514 cm^{-1}) peaks[27].
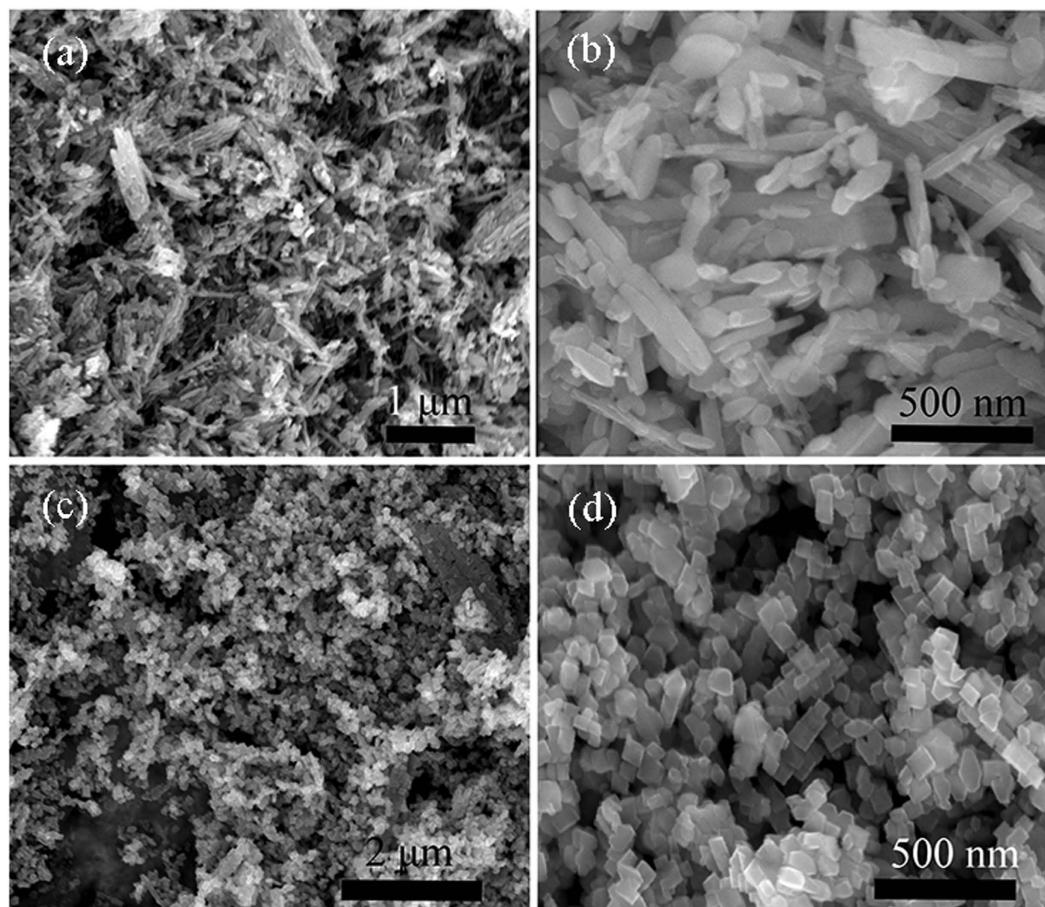
Figure 2. SEM images of the as-prepared TiO$_2$. (**a**,**b**) Without NH$_4$F, the obtained TiO$_2$ nanostructures were random shapes. (**c**,**d**) With NH$_4$F, regular TiO$_2$ nanoparticles were obtained.

Figure 2 shows typical scanning electron microscopy (SEM) images of the TiO$_2$ synthesized in pure water and in NH$_4$F solution. After hydrothermal reaction and washing with HCl solution, the morphology of the as-prepared H$_2$Ti$_5$O$_{11}$·H$_2$O was nanowire structure (Fig. 1S in Supplementary Information). After the further hydrothermal treatment at 200 °C for 48 h, the morphology of the H$_2$Ti$_5$O$_{11}$·H$_2$O nanowires undergone significant change. The H$_2$Ti$_5$O$_{11}$·H$_2$O nanowires were decomposed into random shape TiO$_2$ nanostructures in pure water, as shown in Fig. 2 (a,b). There was complex morphology of nanorod, nanosphere, nanoellipsoid, irregular nanostructures, *etc.* Interestingly, the morphology of the TiO$_2$ obtained in NH$_4$F solution was regular nanoparticles with size of ~50 nm as illustrated in Fig. 2(c,d), in good agreement with the XRD measurement. The NH$_4$F as morphology controlling agent led the H$_2$Ti$_5$O$_{11}$·H$_2$O nanowires to completely decomposing into regular TiO$_2$ nanopaticles[27].

The transmission electron microscopy (TEM) was used to further characterize the crystal structure and morphology of H$_2$Ti$_5$O$_{11}$·H$_2$O and TiO$_2$ nanostrctures in Figure 3. Fig. 3(a,b) shows the H$_2$Ti$_5$O$_{11}$·H$_2$O nanowire sample. The lattice fringes with distances of 0.940 nm in the HRTEM image of Fig. 3(b) corresponded well with (200) plane of H$_2$Ti$_5$O$_{11}$·H$_2$O phase. Figure 3(c) shows TEM image of random shape TiO$_2$ nanostructures by the further hydrothermal reaction in pure water. The HRTEM image (Fig. 3(d)) corresponding the dark red-box area shows interplanar spacing of 0.352 nm, which matches well with (101) plane of anatase TiO$_2$. When the second-step hydrothemal reaction was taken in NH$_4$F solution, the H$_2$Ti$_5$O$_{11}$·H$_2$O nanowires were decomposed into regular TiO$_2$ nanopaticles (Fig. 3(e)). The HRTEM image corresponding the cyan-box area in Fig. 3(e) was revealed in Fig. 3(f), where the interplanar spacing of 0.192 and 0.237 nm corresponded to (200) and (004) planes of anatase TiO$_2$, respectively. In addition, the (004) plane indicated the anatase TiO$_2$ single crystal with exposed {001} facets, and the shape of anatase TiO$_2$ was truncated octahedron. Further, the {101} facets could be also observed through TEM technique (Fig. 2S in Supplementary Information).

Growth mechanism. Figure 4 illustrates the schematic of the preparation process of random shape TiO$_2$ nanostrctures and truncated octahedron TiO$_2$ nanoparticles with exposed {001} facets *via* a two-step hydrothermal reaction process. At the first-step hydrothermal reaction, Ti powder reacted with NaOH to synthesize Na-titanate nanowires. Followed by washing with diluted HCl solution, the
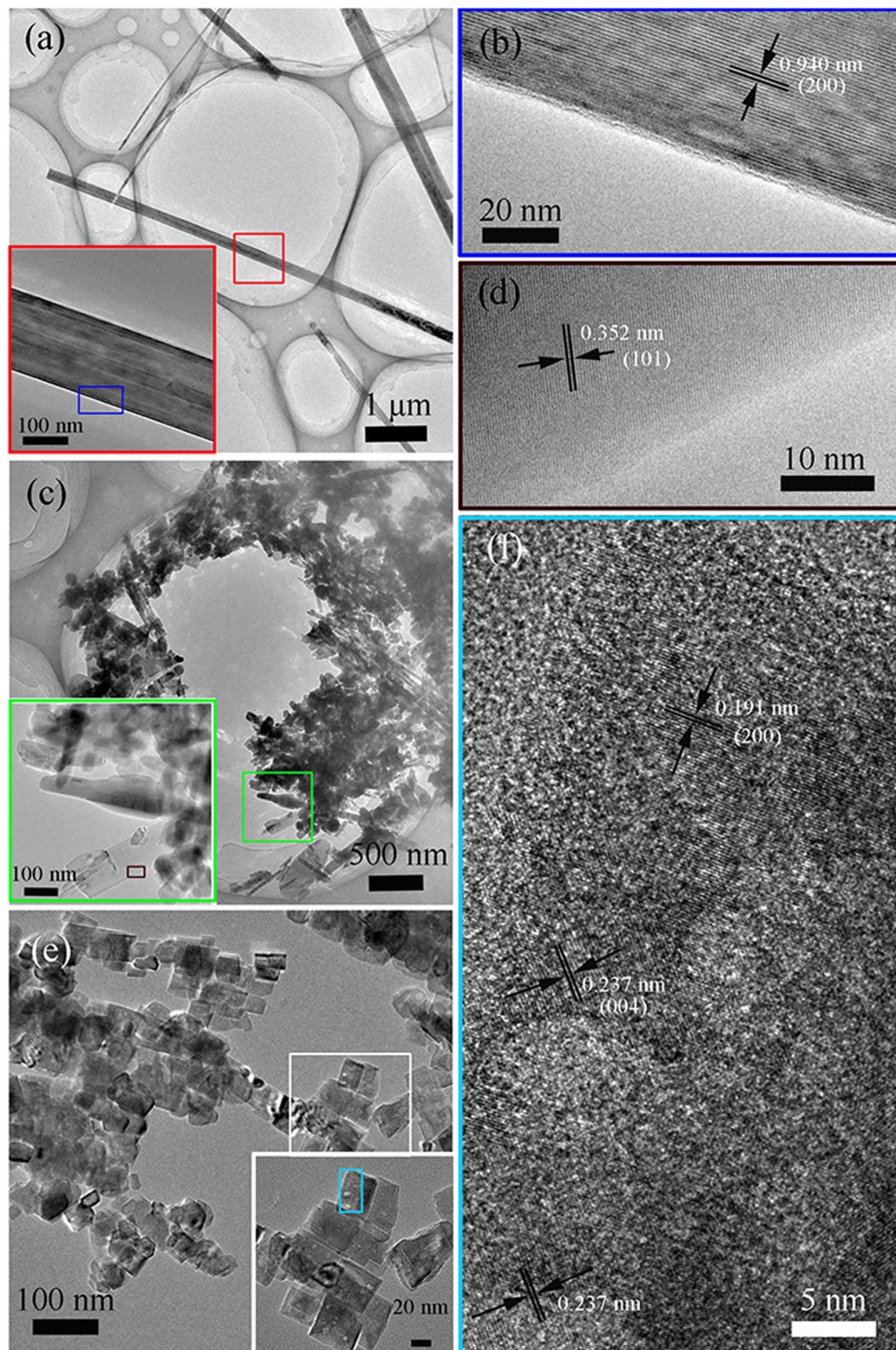
Figure 3. TEM and HRTEM images of the as-prepared samples. (a,b) H-titanate nanowires, (c, d) random shape TiO_2 nanostructures obtained in pure water, (**e,f**) truncated octahedron TiO_2 nanoparticles obtained in NH_4F solution.

Na-titanate nanowires were transformed into H-titanate nanowires *via* cation exchange reaction. At the second-step hydrothermal reaction, the H-titanate nanowires precursors was under gone completely change in aqueous solution with or without NH_4F. In this process, the H-titanate precursors experienced
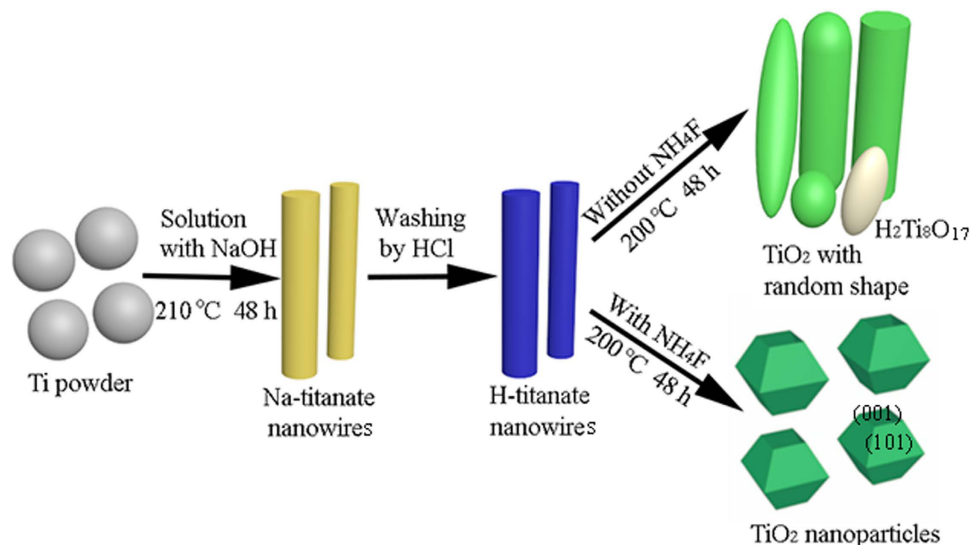
Figure 4. Schematic illustration of the synthetic route of TiO$_2$. In pure water, random shape anatase TiO$_2$ with few H$_2$Ti$_8$O$_{17}$ and rutile TiO$_2$ nanostrutures were formed. While in the present of NH$_4$F, truncated octahedron TiO$_2$ nanoparticles with exposed {001} facets were obtained.

a dissolution and nucleation process during the hydrothermal treatment[28]. In pure water, the dissolution occurred without any restraint, thus TiO$_2$ nanostructures with random shape distribution were obtained. Moreover, the nucleation was not thorough, and there was few H$_2$Ti$_8$O$_{17}$ phase and TiO$_2$ rutile phase. When the H-titanate precursors were performed dissolution and nucleation in NH$_4$F solution, single crystal anatase TiO$_2$ nanoparticles with exposed {001} facets were obtained. At the dissolution process, the existing of F$^-$ ions could be bonded with Ti atom to reduce the surface energy of the {001} facets to lower than that of the {101} facets, resulting in exposing {001} facets during nucleation[29,30]. Besides, F$^-$ ions acted as morphology controlling agent to control the shape of TiO$_2$ nanostructures during nucleation, and the shape of TiO$_2$ nanoparticles was truncated octahedron, as shown in Fig. 4.

Characterization of Photovoltaic Performance. The obtained TiO$_2$ powders were mixed with some additive agents to make TiO$_2$ pastes, and then the TiO$_2$ pastes were coated on TiCl$_4$-treated FTO glasses by doctor-blading method to realize photoanodes after annealing. The thickness of the TiO$_2$ photoanodes was 13.5 μm (Fig. 3S in Supplementary Information). Figure 5(a) indicates the current density-voltage (I-V) curves of the DSSCs based on random shape TiO$_2$ nanostructures (noted "Without F$^-$") and truncated octahedron TiO$_2$ nanoparticles with 34% exposed {001} facets (noted "With F$^-$"). Table 1 listed the corresponding detailed photovoltaic parameters, including the open-circuit voltage (V_{OC}), short-circuit current density (J_{SC}), fill factor (FF), and PEC. The larger PCE 7.06% of DSSCs (noted "With F$^-$") was mainly rooted in the J_{SC}, which increased from 6.86 to 14.80 mA/cm^2. Generally, J_{SC} can be approximated as following expression[31]:

$$J_{sc} = e\eta_{1h}\eta_{inj}\eta_{cc}I_0 \qquad (1)$$

where e is the elementary charge, η_{lh} is the light-harvesting efficiency related to the amount of adsorbed dye molecules and the light-scattering properties, η_{inj} is the charge-injection efficiency, η_{cc} is the charge-collection efficiency relied on competition between charge recombination and collection, and I_0 is the light flux. Here, η_{inj} is suggested to be of the same value, because of the injection both from the TiO$_2$ material to N719 dye.

Electrochemical impedance spectroscopic (EIS) measurements were conducted in the dark under a bias of 0.75 V to evaluate the charge transfer and recombination as the Nyquist plots in Fig. 5(b)[32]. The radius of semicircle in Nyquist plots revealed the charge-transfer resistance (R_{ct}) between TiO$_2$/dye/electrolyte interfaces. The slightly larger one based on the random shape TiO$_2$ nanostructures (Without F$^-$) indicated a slow charge recombination at the TiO$_2$/dye/electrolyte interfaces. Namely, the electron lifetime in photoanodes based on the random shape TiO$_2$ nanostructures was slightly longer. Moreover, the electron lifetime (τ) was calculated using the following equation[33,34]:

$$\tau = R_{ct}C_u \qquad (2)$$

where C_u is the corresponding chemical capacitance. The corresponding values of R_{ct} (243.3 and 237.1 Ω) and C_u (7.5534 × 10^{-4} and 7.1165 × 10^{-4} F) can be obtained by simulation using the Zview software. The
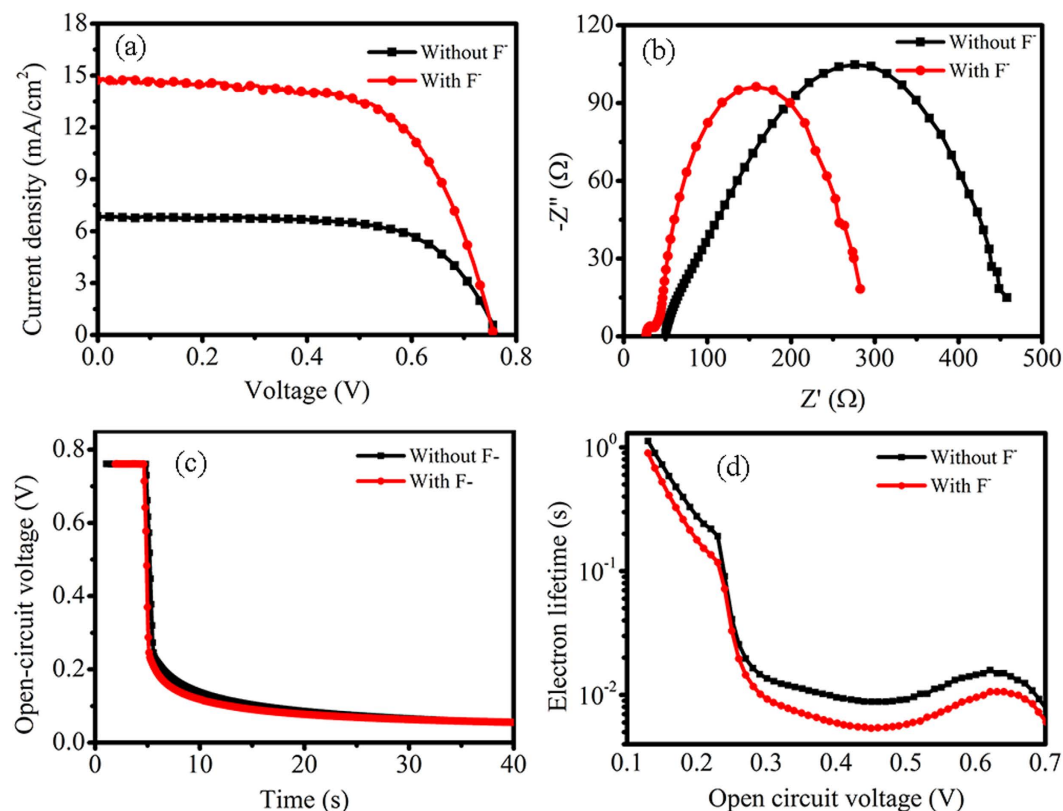
Figure 5. Photovoltaic characteristics of the DSSCs based on random shape TiO$_2$ nanostructures (noted "Without F$^-$") and truncated octahedron TiO$_2$ nanoparticles with exposed {001} facets (noted "With F$^-$"). (**a**) I-V curves. (**b**) Nyquist plots by EIS measurements. (**c**) Open-voltage decay measurement upon turning off the illumination. (**d**) Electron lifetime determined from the data of (**c**).

Samples	J_{sc} (mA/cm^2)	V_{oc}(V)	FF	PCE	Adsorbed dye (nmol/cm^2)[a]
Without F$^-$	6.86	0.764	0.662	3.47%	32.6
With F$^-$	14.80	0.756	0.631	7.06%	122.9

Table 1. Photovoltaic parameters of the DDSCs based on random shape TiO$_2$ nanostructures (noted "Without F$^-$") and truncated octahedron TiO$_2$ nanoparticles with 34% exposed {001} facets (noted "With F$^-$"). [a]Dye-adsorbed films with a dimension of 0.9 cm^2 were used for estimating the adsorbed dye concentration.

electron lifetime was 0.184 (Without NH$_4$F) and 0.179 s (With F$^-$) of DSSCs, respectively. Meanwhile, the open-voltage decay method was employed to further investigate the electron lifetime of the two cells, as shown in Fig. 5(c). From the open-voltage decay rate, the electron lifetime (τ) can be calculated by the following equation[35,36]:

$$\tau = -\left(\frac{k_B T}{e}\right)\left(\frac{dV_{OC}}{dt}\right)^{-1}$$

(3)

where k_B is the Boltzmann constant, and T is room temperature. The calculated data of τ were plotted in Fig. 5(d). It was observed that the electron lifetime based on random shape TiO$_2$ nanostructures was slightly longer than that based on TiO$_2$ nanoparticles. The possible reason was that there were some nanorods and relatively large nanoparticles in random shape TiO$_2$ nanostructures, which were in favour of charge transfer. Therefore, it dos no outstanding difference to the charge transfer, and the value of η_{cc} of DSSCs (noted "Without NH$_4$F") was little larger than that one (noted "With NH$_4$F"). In other words, the increasing of J_{SC} at over twice was not from the factor of η_{cc}.
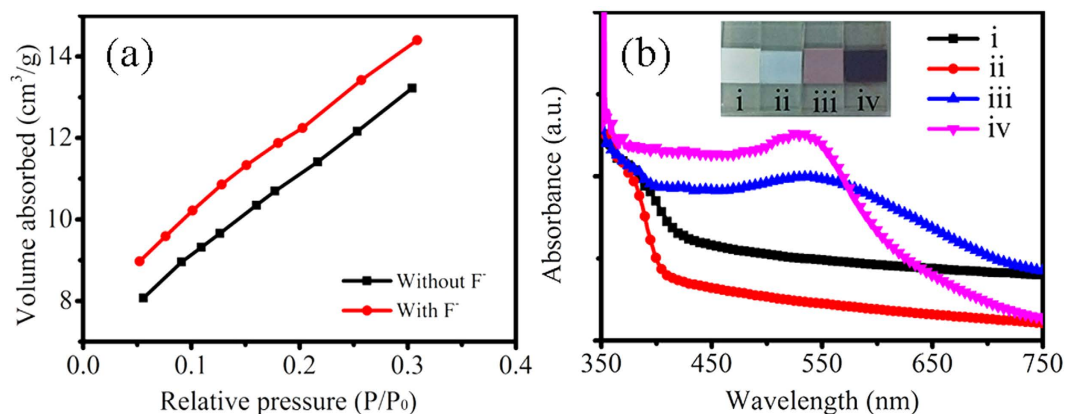
Figure 6. N$_2$ adsorption isotherms and absorption spectra. (**a**) N$_2$ adsorption isotherms of random shape TiO$_2$ nanostructures (noted "Without F$^-$") and truncated octahedron TiO$_2$ nanoparticles (noted "With F$^-$"). (**b**) UV-Vis absorption spectrum of random shape TiO$_2$ nanostructure films (without/with sensitizing, i/iii) and truncated octahedron TiO$_2$ nanoparticle films (without/with sensitizing, ii/iv) on FTO substrates. The inset shows optical images of TiO$_2$ films (without/with sensitizing) on FTO substrates.

It is well-known that the nanoparticle films have large special surface area to load more dye molecules[1]. Therefore, the special surface area was checked by Brunauer-Emmett-Teller (BET) data as shown in Fig. 6(a). The BET surface area was measured as 40.9 and 44.6 m^2/g for random shape TiO$_2$ nanostructures and TiO$_2$ nanoparticles, respectively. The special surface area of TiO$_2$ nanoparticles was slightly bigger than that of the random shape TiO$_2$ nanostructures. More importantly, exposing highly reactive {001} facets of TiO$_2$ can enhance dye adsorption[17]. Thus, we investigated the amount of absorbed dye molecules to elucidate the factor of η_{lh}. The optical image of TiO$_2$ and sensitized-TiO$_2$ films on FTO substrates was shown as the inset in Fig. 6(b). The color of random shape TiO$_2$ nanostructure films (i) was lutescent, while the color of TiO$_2$ nanoparticle films (ii) was pure white. After being sensitized by N719 dye, the color of the sensitized-TiO$_2$ films based on TiO$_2$ nanoparticles (iv) was darker red than that of based on random shape TiO$_2$ nanostructures (iii), indicating that the TiO$_2$ nanoparticles with exposed {001} facets absorbed more dye molecules. The UV-vis absorbance measurements in Fig. 6(b) revealed the sensitized-TiO$_2$ films based on TiO$_2$ nanoparticles (iv) had a stronger visible absorption, because of more amount of loading dye molecules. The absorbed dye amounts were calculated from UV-vis absorbance measurements of the concentration desorbed N719 dye in NaOH solution by using Lambert-Beer's Law[37,38]. The absorbed dye amount of photoanodes based on TiO$_2$ nanopartiles with exposed {001} facets was about four times than that of based on random shape TiO$_2$ nanostructures, as listed in Table 1. The TiO$_2$ nanoparticles with exposed {001} facets had excellent capacity for adsorption of dye molecules. As a consequence, anatase TiO$_2$ nanoparticles with exposed {001} facets were efficient photoanodes for DSSCs.

Discussion

Anatase TiO$_2$ nanoparticles with 34% exposed {001} facets have been successfully synthesized from Ti powder *via* two-step hydrothermal reaction process. The first -step hydrothermal reaction was alkaline hydrothermal reaction to obtain H-titanate nanowires. At the second-step hydrothermal reaction, the H-titanate nanowires were decomposed into random shape anatase TiO$_2$ nanostrctures with few impurity in pure water or truncated octahedron anatase TiO$_2$ nanopaticles with 34% exposed {001} facets in NH$_4$F solution. The DSSCs based on anatase TiO$_2$ nanopaticles with 34% exposed {001} facets showed outstanding performance of efficiency 7.03%, which was about twice than that of based on random shape TiO$_2$ nanostructures. The high performance was ascribed to that the anatase TiO$_2$ nanopaticles with 34% exposed {001} facets own high activity and large special surface area for excellent capacity of absorbing dye molecules. We anticipate that the anatase TiO$_2$ nanopaticles with 34% exposed {001} facets open up a promising avenue for efficient TiO$_2$-based photoelectric nanodevices.

Methods

Materials. Fuorinated tin oxide (FTO, ~7 Ω/cm^2) glasses were bought from Nippin Sheet Glass Co., Ltd. Sodium hydroxide (NaOH, 96.0%), titanium tetrachloride (TiCl$_4$, 99.0%), ammonium fluoride (NH$_4$F, 96.0%), hydrochlriic acid (HCl, 36%~38%wt), ethanol (99.7%) and acetone (99.5%) were purchased from Sinopharm Chemical Reagent Co. Ltd. Ruthenium 535-bisTBA (N719) was purchased from Solaronix. Guanidinium thiocyanate (GuSCN, 99.0%) was from Amresco. Titanium powder (Ti, 99.99%), lithium iodide (LiI, 99.999%), iodine (I$_2$, 99.99%), 1-methyl-3- propylimidazolium iodide (PMII, 98%), 4-tert-butylpyridine (4-TBP, 96%) and tert-butyl alcohol (99.5%) were obtained from

Aladdin. Acetonitrile (99.8%) and valeronitrile (99%) were from Alfa Aesar. All solvents and chemicals were reagent grade and were used without further purification.

Synthesis of H-titanate nanowires.

Na-titanate nanowires were firstly synthesized by alkali hydrothermal reaction of Ti powder in NaOH solution. First, 70 mL of 10 M NaOH solution was obtained under magnetic stirring. Then 0.2 g Ti powder was added into the above NaOH solution and stirred for 10 minimums again. The final solution was transferred to a 100 ml Teflon-lined stainless steel autoclave and loaded into an oven. The temperature was set 210 °C for 48 hours and then cooled down to room temperature naturally. After the hydrothermal treatment, the obtained Na-titanate nanowires were completely washed with 0.1 M HCl solution to replace Na^+ with H^+. Subsequently, the H-titanate nanowires were washed with deionized water several times.

Synthesis of anatase TiO_2 nanopaticles with exposed {001} facets.

The above total H-titanate nanowires were added into 100 mL Teflon-lined stainless steel autoclave containing 70 ml deionized water with or without adding 0.25 M NH_4F. Afterward, the autoclave was loaded into an oven at 200 °C for 48 hours and then cooled down to room temperature naturally. After the hydrothermal reaction, the obtained TiO_2 powders were collected from the solution, and washed with deionized water and ethanol for several times by centrifugation. Finally, the powders were dried at 80 °C over night. The obtained dry powder was anatase TiO_2 nanopaticles with exposed {001} facets in NH_4F solution or random shape TiO_2 nanostuctures with few impurity in pure water.

Preparation of TiO_2 photoanode.

1 g TiO_2 powder was mixed evenly under magnetic stirring in a mixture of 0.2 mL acetic acid, 3.0 g terpineol, 0.5 g ethyl cellulose and some ethanol to form a slurry, the slurry was milled in a mortar for about 20 min, and then dispersed with ultrasonic for 10 min to prepare viscous white TiO_2 paste. The FTO glasses were washed with detergent and sonicated in deionized water, acetone and ethanol for 20 min, respectively. After dried under flowing argon gas, the cleaned FTO glasses were soaked into 0.04 M $TiCl_4$ solution at 70 °C for 30 min to form a compact TiO_2 layer, and then rinsed with deionized water and ethanol. The TiO_2 pastes were printed onto the $TiCl_4$-treated FTO glasses by doctor-blading method. Then the printed TiO_2 layers were annealed at 125 °C for 15 min, at 325 °C for 5 min, at 375 °C for 5 min, at 450 °C for 15 min, and then at 500 °C for 15 min in a muffle furnace. The annealed TiO_2 layers were immersed into 40 mM $TiCl_4$ solution at 70 °C for 30 min again, and after being rinsed with deionized water and ethanol, the films were sintered at 500 °C for 30 min in muffle furnace. After the temperature was cooled to about 80 °C, the TiO_2 pohtoanodes were immersed into 0.5 mM N719 dye in acetonitrile/tert-butanol (V:V/1:1), and kept for 16 h at room temperature. The sensitized TiO_2 photoanodes were washed with acetonitrile to remove the possible physically-adsorbed dye molecules.

Fabrication of DSSCs.

The Pt counter electrodes were deposited by magnetron sputtering on cleaned FTO glasses. Sputtering was performed using a Pt (99.99% purity) target in an Ar ambient atmosphere at 100 W. For fabricating DSSCs, the Pt counter electrodes were buckled on the sensitized-TiO_2 photoanodes, which were sealed using a 50 μm plastic sheet and the internal space was filled with a liquid electrolyte. The electrolyte was composed of 0.6 M PMII, 0.05 M LiI, 0.03 M I_2, 0.1 M GuSCN and 0.5 M 4-TBP in acetonitrile and valeronitrile (V:V/85:15). The active area of the solar cell was 0.15 cm² without a mask.

Measurement.

The crystal structure and phase purity of the obtained powders were investigated using a powder X-ray diffractometer (XRD, PANalytical B.V., The Netherlands) with Cu-Kα ($\lambda = 0.15418$ nm) radiation. Raman measurement was carried out using a Raman spectroscopy (LABRAM HR800, France) with a 514.5 nm argon ion laser of 200 μm spot size for excitation. The size and morphology of the samples were recorded by field emission scanning electron microscopy (SEM, FEI NOVA NanoSEM 450). Transmission electron microscopy (TEM) and and high-resolution TEM (HRTEM) images were performed by TEM (FEI Tecnai G^2 20 UTwin) or aberration-corrected TEM (FEI Titan G^2 60-300). The sample was prepared by drop casting ethanolic dispersion of tiny TiO_2 powder onto a carbon coated Cu grid. The Brunauer-Emmett-Teller (BET, V-Sorb 2800P) was carried out to measure the surface area of the samples. The current density-voltage (*I-V*) measurements, open-voltage decay measurements, and electrochemical impedance spectroscopy (EIS) measurements were performed by an Autolab electrochemic workstation (modelAUT84315, The Netherlands). UV-Vis absorption spectrometry (UV-2550, Shimadzu) was employed to test the absorption spectra. The illumination intensity was AM 1.5G (100 mW/cm², calibrated with a Si photodiode) using a solar simulator (Newport, USA). The electrochemical impedance spectroscopy (EIS) measurements were scanned in dark condition at a bias of 0.75 V with an amplitude of 10 mV in a frequency range from 100 kHz to 0.1 Hz. For testing the adsorbed dye amount of the TiO_2 working eletrodes, the sensitized-TiO_2 samples desorbed the dye into 0.1 M NaOH solution. The measured absorption spectra were used to calculate the amount of the adsorbed dye amount, expressed in terms of moles of dye anchored per projected unit area of the photoanodes.

References

1. O'Regan, B. & Gratzel, M. A low-cost, hight-efficiency solar cell based on dye-sensitized colloidal TiO$_2$ film. *Nature* **353,** 737–740 (1991).
2. Hagfeldt, A., Boschloo, G., Sun, L. C., Kloo, L. & Pettersson, H. Dye-sensitized solar cells. *Chem. Rev.* **110,** 6595–6663 (2010).
3. Yella, A. *et al.* Electrolyte exceed 12 percent efficiency based redox-porphyrin-sensitized solar cells with cobalt (II/III). *Science* **334,** 629–634 (2011).
4. Yanagida, S., Yu, Y. H. & Manseki, K. Iodide-free dye-sensitized solar cells. *Acc. Chem. Res.* **42,** 1827–1838 (2009).
5. Hardin, B. E., Snaith, H. J. & McGehee, M. D. The renaissance of dye-sensitized solar cells. *Nature Photonics* **6,** 162–169 (2012).
6. Ahmad, S. *et al.* Metal free sensitizer and catalyst for dye sensitized solar cells. *Energy Environ. Sci.* **6,** 3439–3466 (2013).
7. Chiba, Y. *et al.* Dye-sensitized solar cells with conversion efciency of 11.1%. *Jpn. J. Appl. Phys.* **45,** 638–640 (2006).
8. Sun, Z., Kim, J. H., Zhao, Y., Attard, D., Dou, S. X. Morphology-controllable 1D-3D nanostructured TiO$_2$ bilayer photoanodes for dye-sensitized solar cells. *Chem. Commun.* **49,** 966–968 (2013).
9. Crossland, E. J. W. *et al.* Mesoporous TiO$_2$ single crystals delivering enhanced mobility and optoelectronic device performance. *Nature* **495,** 215–220 (2013).
10. Wu, W. Q. *et al.* Morphology-controlled cactus-like branched anatase TiO$_2$ arrays with high light-harvesting efficiency for dye-sensitized solar cells. *J. Power Sources* **260,** 6–11 (2014).
11. Chen, X. B. & Mao, S. S. Titanium dioxide nanomaterials: synthesis, properties, modifications, and applications. *Chem. Rev.* **107,** 2891–2959 (2007).
12. Li, W., Wu, Z. X., Wang, J. X., Elzatahry, A. A. & Zhao, D. Y. A perspective on mesoporous TiO$_2$ materials. *Chem. Mater.* **26,** 287–298 (2014).
13. Lee, J. W., Lee, J., Kim, C., Cho, C. Y. & Moon, J. H. Facile fabrication of sub-100 nm mesoscale inverse opal films and their application in dye-sensitized solar cell electrodes. *Sci. Rep.* **4** (2014).
14. Liao, J. Y., Lei, B. X., Kuang, D. B. & Su, C. Y. Tri-functional hierarchical TiO$_2$ spheres consisting of anatase nanorods and nanoparticles for high efficiency dye-sensitized solar cells. *Energy Environ. Sci.* **4,** 4079–4085 (2011).
15. Park, N. G., van de Lagemaat, J. & Frank, A. J. Comparison of dye-sensitized rutile-and anatase-based TiO$_2$ solar cells. *J. Phys. Chem. B* **104,** 8989–8994 (2000).
16. Chen, C. D. *et al.* Microwave-assisted topochemical conversion of layered titanate nanosheets to {010}-faceted anatase nanocrystals for high performance photocatalysts and dye-sensitized solar cells. *Cryst. Growth Des.* **14,** 5801–5811 (2014).
17. Wu, X., Chen, Z. G., Lu, G. Q. & Wang, L. Z. Nanosized anatase TiO$_2$ single crystals with tunable exposed (001) facets for enhanced energy conversion efficiency of dye-sensitized solar cells. *Adv. Funct. Mater.* **21,** 4167–4172 (2011).
18. Fang, W. Q., Gong, X. Q. & Yang, H. G. On the unusual properties of anatase TiO$_2$ exposed by highly reactive facets. *J. Phys. Chem. Lett.* **2,** 725–734 (2011).
19. Chen, J. S. *et al.* Constructing hierarchical spheres from large ultrathin anatase TiO$_2$ nanosheets with nearly 100% exposed (001) facets for fast reversible lithium storage, *J. Am. Chem. Soc.* **132,** 6124–6130 (2010).
20. Jung, M. H., Chu, M. J. & Kang, M. G. TiO$_2$ nanotube fabrication with highly exposed (001) facets for enhanced conversion efficiency of solar cells. *Chem. Commun.* **48,** 5016–5018 (2012).
21. Yu, J. G. *et al.* Anatase TiO$_2$ nanosheets with exposed (001) facets: improved photoelectric conversion efficiency in dye-sensitized solar cells. *Nanoscale* **2,** 2144–2149 (2010).
22. Fang, W. Q. *et al.* Yolk@shell anatase TiO$_2$ hierarchical microspheres with exposed {001} facets for high-performance dye sensitized solar cells. *J. Mater. Chem.* **22,** 22082–22089 (2012).
23. Yu, J. G. *et al.* Enhanced photocatalytic CO$_2$-reduction activity of anatase TiO$_2$ by coexposed {001} and {101} facets. *J. Am. Chem. Soc.* **136,** 8839–8842 (2014).
24. Laskova, B. *et al.* Electron kinetics in dye sensitized solar cells employing anatase with (101) and (0 01) facets. *Electrochimica Acta* **160,** 296–305 (2015).
25. Mathew, S. *et al.* Dye-sensitized solar cells with 13% efficiency achieved through the molecular engineering of porphyrin sensitizers. *Nature Chem.* **6,** 242–247 (2014).
26. Tao, J., Dong, X., Zhu, H., Tao, H. J., He, P. T. Enhanced photocatalytic properties of ultra-long nanofiber synthesized from pure titanium powders. *Rare Metals* **31,** 39–42 (2012).
27. Tian, F., Zhang, Y. P., Zhang, J. & Pan C. X. Raman spectroscopy: a new approach to measure the percentage of anatase TiO$_2$ exposed (001) facets. *J. Phys. Chem. C* **116:13,** 7515–7519 (2012).
28. You, T., Jiang, L., Han, K. L. & Deng, W. Q. Improving the performance of quantum dot-sensitized solar cells by using TiO$_2$ nanosheets with exposed highly reactive facets. *Nanotechnology* **24,** 245401–6 (2013).
29. Li, H. M. *et al.* Hierarchical TiO$_2$ nanospheres with dominant {001} facets: facile synthesis, growth mechanism, and photocatalytic activity. *Chem. Eur. J.* **18,** 7525–7532 (2012).
30. Yang, H. G. *et al.* Anatase TiO$_2$ single crystals with a large percentage of reactive facets. *Nature* **453,** 638–642 (2008).
31. Zhu, K., Neale, N. R., Miedaner, A. & Frank, A. J. Enhanced charge-collection efficiencies and light scattering in dye-sensitized solar cells using oriented TiO$_2$ nanotubes arrays. *Nano Lett.* **7:1,** 69–74 (2007).
32. Liao, J. Y., Lin, H. P., Chen, H. Y., Kuang, D. B. & Su, C. Y. High-performance dye-sensitized solar cells based on hierarchical yolk-shell anatase TiO$_2$ beads. *J. Mater. Chem.* **22,** 1627–1633 (2012).
33. Tian, J. J. *et al.* Architectured ZnO photoelectrode for high efciency quantum dot sensitized solar cells. *Energy Environ. Sci.* **6,** 3542–3547 (2013).
34. Wang, Q. *et al.* Characteristics of high efficiency dye-sensitized solar cells. *J. Phys. Chem. B* **110,** 25210–25221 (2006).
35. Zaban, A., Greenshtein, M. & Bisquert, J. Determination of the electron lifetime in nanocrystalline dye solar cells by open-circuit voltage decay measurements. *Chem. Phys. Chem.* **4,** 859–864 (2003).
36. Bisquert, J., Zaban, A., Greenshtein, M. & Mora-Seró, I. Determination of rate constants for charge transfer and the distribution of semiconductor and electrolyte electronic energy levels in dye-sensitized solar cells by open-circuit photovoltage decay method. *J. Am. Chem. Soc.* **126,** 13550–13559 (2004).
37. Wang, Z. S., Kawauchi, H., Kashima, T. & Arakawa, H. Significant influence of TiO$_2$ photoelectrode morphology on the energy conversion efficiency of N719 dye-sensitized solar cell. *Coord. Chem. Rev.* **248,** 1381–1389 (2004).
38. Jang, I., Song, K., Park, J. H. & Oh, S. G. Enhancement of dye adsorption on TiO$_2$ surface through hydroxylation process for dye-sensitized solar cells. *Bull. Korean Chem. Soc.* **34,** 2883–2888 (2013).

Acknowledgements

Author Contributions

L.C. carried out all experiments, devised the original concept, and wrote the draft of the manuscript; Z.F.Q. participated in discussion of results; J.P.Y. & X.A.L. discussed the interpretation of results and revised the manuscript. All authors discussed the results and participated in manuscript revision. J.P.Y. & X.A.L. are corresponding authors.

Additional Information

Supplementary information accompanies this paper at http://www.nature.com/srep

Competing financial interests: The authors declare no competing financial interests.

How to cite this article: Chu, L. *et al.* Anatase TiO_2 Nanoparticles with Exposed {001} Facets for Efficient Dye-Sensitized Solar Cells. *Sci. Rep.* **5**, 12143; doi: 10.1038/srep12143 (2015).